Theory input for $t\bar{t}j$ experimental analyses at the LHC

Maria Vittoria Garzelli[1], Adrian Irles[2], Sven-Olaf Moch[1], Peter Uwer[3] and Katharina Voß[1,4]

[1]Universität Hamburg, [2]IFIC - CSIC & University of Valencia, [3]Humboldt-Universität Berlin, [4]Universität Siegen

Matter To The Deepest 2021
15. September 2021

Studying the top quark at the LHC

fundamental particle with the largest mass in the SM:
$m_t = 172.76 \pm 0.30\,\text{GeV}$ (direct measurement)
$m_t(m_t) = 162.5^{+2.1}_{-1.5}\,\text{GeV}$ ($\overline{\text{MS}}$ mass, cross section measurements)
$m_t = 172.5 \pm 0.7\,\text{GeV}$ (pole mass, cross section measurements)
[P.A. Zyla et al. (PDG) 2020]

LHC = 'top quark factory':
high statistics enable precise measurements of the top quark processes (precision SM measurements, Higgs-Yukawa, BSM, $\cdots$)

Why is the measurement of the top quark mass interesting?

Radiative corrections to M_W

consistency check of the SM through radiative corrections involving m_t & m_H

Stability of EW vacuum

effective Higgs potential depends on relations between m_H, m_t and α_s

Motivation for study of $t\bar{t}j$

→ **substantial fraction of $t\bar{t}$-events contain a jet**

for jet cut $p_T^j > 40\,\text{GeV}$ & $\sqrt{s} = 13\,\text{TeV}$: 40 % of $t\bar{t}$-events accompanied by a jet [Kraus hep-ph/1608.05296]

→ **dominant background to Higgs production in VBF**

signal: $pp \to Hjj \to W^+W^-jj$ with jj separated in y

background: $pp \to t\bar{t}j \to b\bar{b}W^+W^-j$ with b produced centrally, but j more evenly in y

→ **top quark mass determination through ρ distribution**

$\rho = 2m_0/\sqrt{m^2_{t\bar{t}j}}$ with $m_0 = 170\,\text{GeV}$ [Alioli, Fernandez, Fuster, Irles, Moch, Uwer, Vos hep-ph/1303.6415]

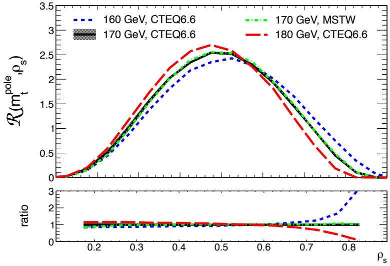

ATLAS [“Measurement of the top-quark mass in $t\bar{t}+$ 1-jet events collected with the ATLAS detector in pp collisions at $\sqrt{s} = 8$ TeV”, hep-ex/1905.02302]

$$m_t^{\text{pole}} = 171.1 \pm 0.4(\text{stat}) \pm 0.9(\text{sys})\,^{+0.7}_{-0.3}(\text{th})\,\text{GeV}$$

theory uncertainty dominated by scale variation uncertainty $(+0.6, -0.2)\,\text{GeV}$ (PDF and α_s uncertainty lead to $\pm 0.2\,\text{GeV}$)

Methods

NLO calculations and POWHEG (Positive Weight Hardest Emission Generator) implementation of $t\bar{t}$ + jet

- NLO calculation of $t\bar{t}$+jet
  stable tops [Dittmaier, Uwer, Weinzierl hep-ph/0810.0452]
  LO top-quark decay [Melnikov, Schulze hep-ph/1004.3284]
  NLO QCD off-shell effects in fully leptonic decay [Bevilacqua, Hartanto, Kraus, Worek hep-ph/1509.09242]
- POWHEL (=HELAC-NLO + POWHEG-BOX) [Kardos, Papadopoulos, Trócsányi hep-ph/1101.2672]
- POWHEG-BOX `ttbarj` [V1 Alioli, Moch, Uwer hep-ph/1110.5251]

Method used in this study: POWHEG-BOX `ttbarj` V2
most important differences for this study to previous V1 version [hep-ph/1110.5251]

- all amplitudes calculated with OpenLoops2
  (V1: Born and real squared amplitudes from MadGraph, virtual from [hep-ph/0810.0452])
- able to parallelize calculation

Scale definitions

Motivation: high-energy tails of NLO differential cross sections in $pp \to t\bar{t}j + X$ in fully leptonic decay better described through dynamical scale definition [Bevilacqua, Hartanto, Kraus, Worek hep-ph/1609.01659]

fixed scale $\mu_0 = m_t$

dyn. scale $\mu_0 \in \{H_T^B/2, H_T^B/4\}, H_T^B = \left(\sqrt{{p_{T,t}^B}^2 + m_t^2} + \sqrt{{p_{T,\bar{t}}^B}^2 + m_t^2} + p_{T,j}^B\right)$

$$\mu_0 = m_{t\bar{t}j}^B/2 = \frac{1}{2}\sqrt{(p_t^B + p_{\bar{t}}^B + p_j^B)^2}$$

^{B} : underlying Born variables

Simulation details: NLO accuracy, $\sqrt{s} = 13\,\text{TeV}$, $m_t = 172\,\text{GeV}$, stable top quarks, (PDF+α_s) CT18NLO, 7 point scale variation with $\mu_{R/F} = K_{R/F}\mu_0$, $(K_R, K_F) \in \{(0.5, 0.5), (0.5, 1), (1, 0.5), (1, 1), (1, 2), (2, 1), (2, 2)\}$

Analysis details: $N_j \geq 1$, $p_T^j > 30\,\text{GeV}$, $|\eta_j| < 2.4$, anti-k_T jet clustering algorithm with $R = 0.4$

Integrated cross section with analysis cuts

$$\mu_0 = m^B_{t\bar{t}j}/2$$

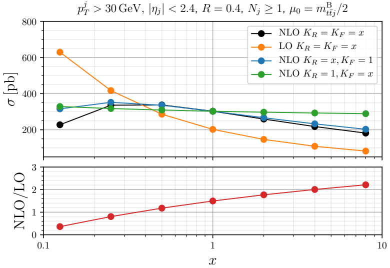

$$\mu_0 = m_t$$

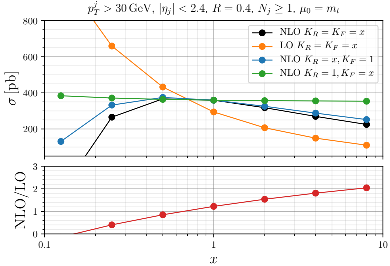

$$\mu_0 = H^B_T/2$$

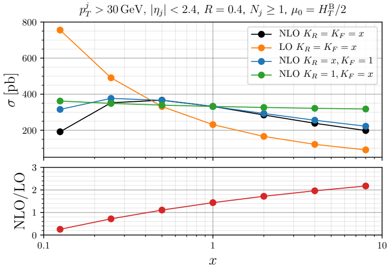

scale variation driven by renormalization scale dependence $(K_R = x, K_F = 1)$

Observation:
NLO/LO ~ 1 for $\mu_R = \mu_F = H^B_T/4$
$\rightarrow$ additional study of this central scale

Scale variation in ρ distribution

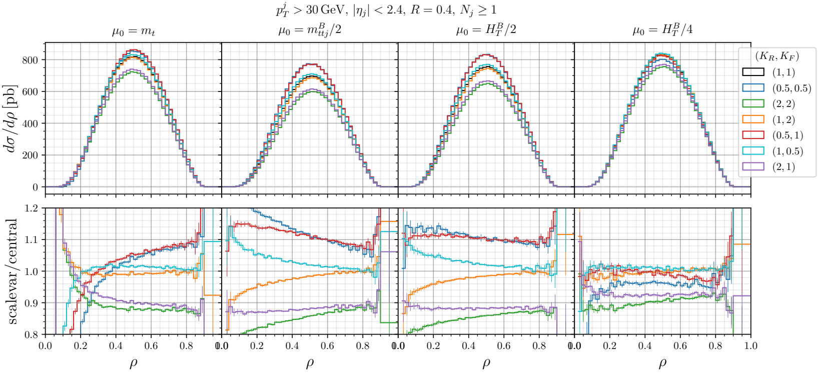

→ large increase in width of scale variation band in high energy tail ($\Leftrightarrow$ small ρ) and crossing of scale variation graphs using fixed scale not seen using dynamical scale

→ varying the scale does not induce large shape variation using a dynamical scale

$$\rho = \frac{2m_0}{m_{t\bar{t}j}}$$

with $m_0 = 170\,\mathrm{GeV}$

Scale variation in normalized ρ distribution at NLO

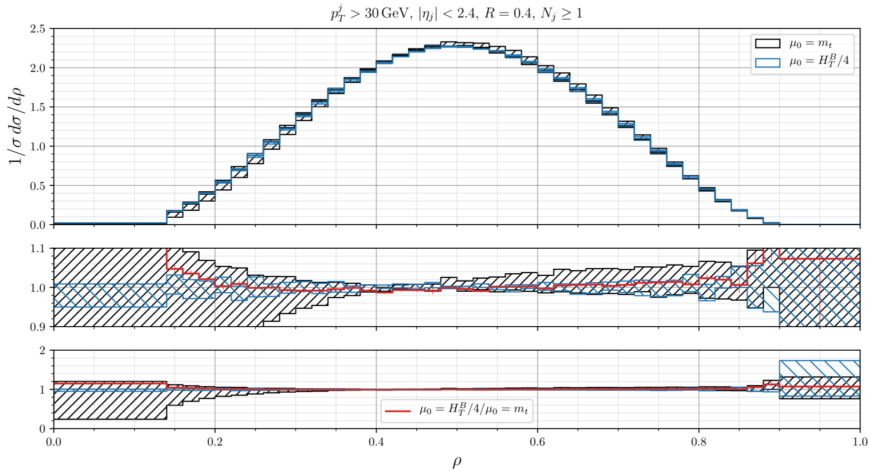

$\rightarrow$ strongly reduced scale uncertainty with $\mu_0 = H_T^B/4$ w.r.t. $\mu_0 = m_t$ due to reduced shape variation of the ρ distribution through scale variation with the dynamical scale

Comparison of the ρ distribution at NLO and LO

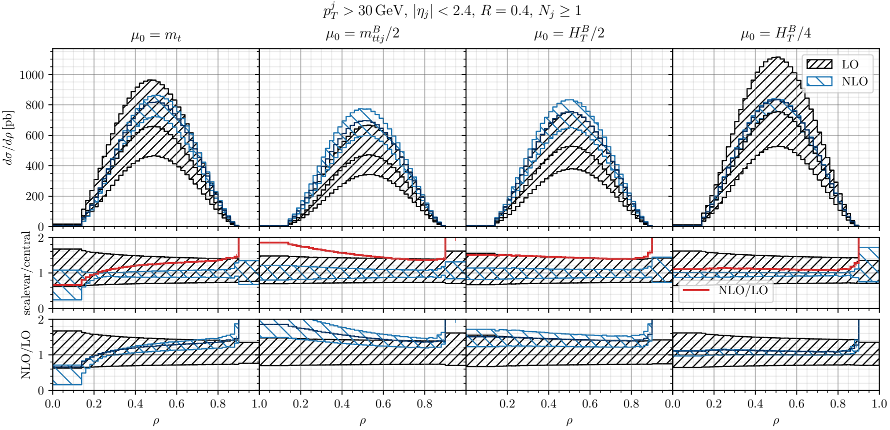

→ shape variation comparing LO and NLO central scale prediction using $\mu_0 = m_t$ and $\mu_0 = m^B_{t\bar{t}j}/2$

→ more uniform differential (NLO/LO) $\mathcal{K}$-factor using $\mu_0 \in \{H^B_T/2, H^B_T/4\}$

Comparison of the $m_{t\bar{t}}$ distribution at NLO and LO

→ reduced width of scale variation uncertainty bands in high energy tails using a dynamical scale instead of a fixed scale already found in [Bevilacqua, Hartanto, Kraus, Worek hep-ph/1609.01659]

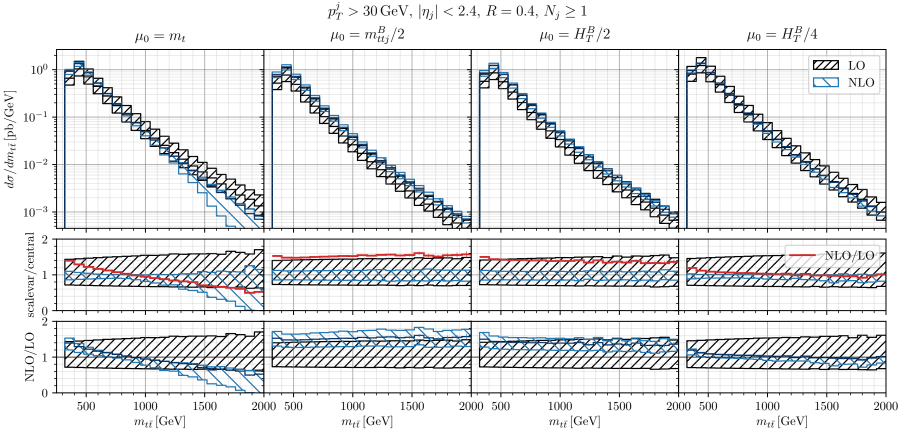

Effect of variation of the R-parameter in ρ distribution

R parameter in anti-k_T algorithm ($R_{ij} = \sqrt{(y_i - y_j)^2 + (\phi_i - \phi_j)^2}$)

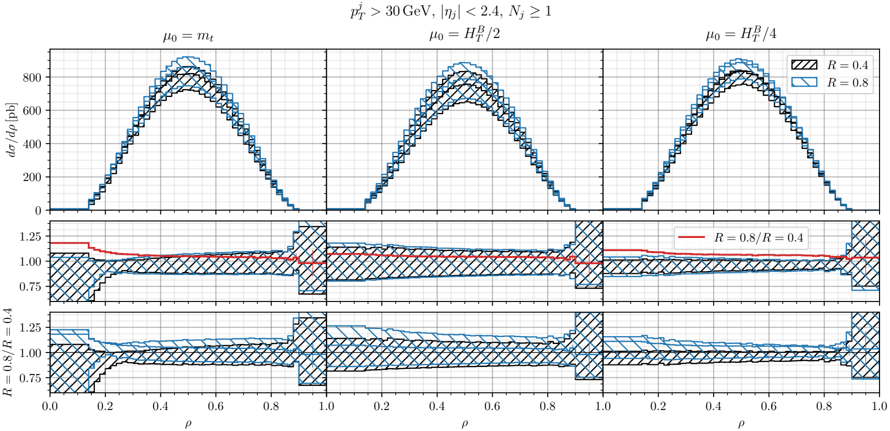

→ larger diff. cross section with $R = 0.8$ compared to $R = 0.4$

→ similar size of scale uncertainty for both R-values with dynamical scale

Effect of variation of the R-parameter in $m_{t\bar{t}}$ distribution

Example: same behaviour observed in other differential distributions

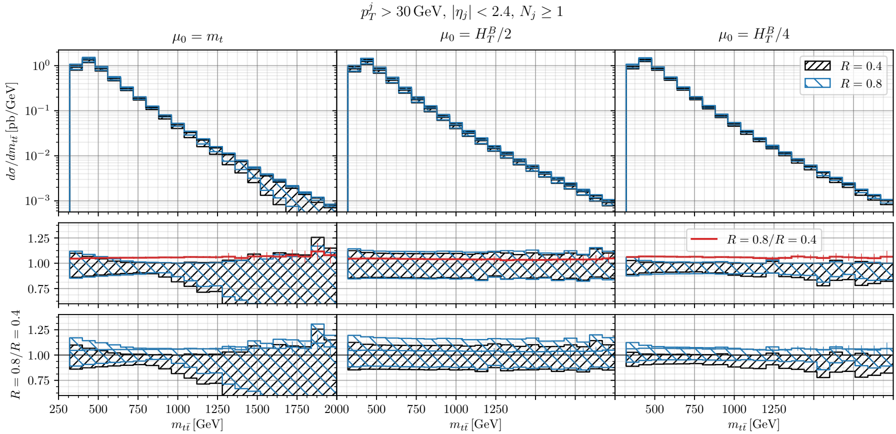

Effect of variation of the R-parameter in p_T^j distribution

Example: same behaviour observed in other differential distributions

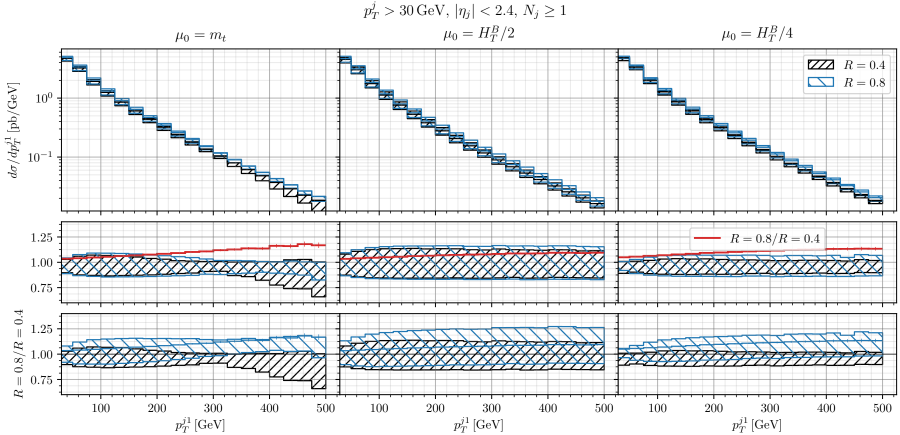

NLO PDF uncertainty within a NLO or LO simulation

Predictions of the PDF uncertainty using the CT18NLO PDF set in association with a NLO or LO partonic cross section using the central scale $\mu_0 = H_T^B/2$

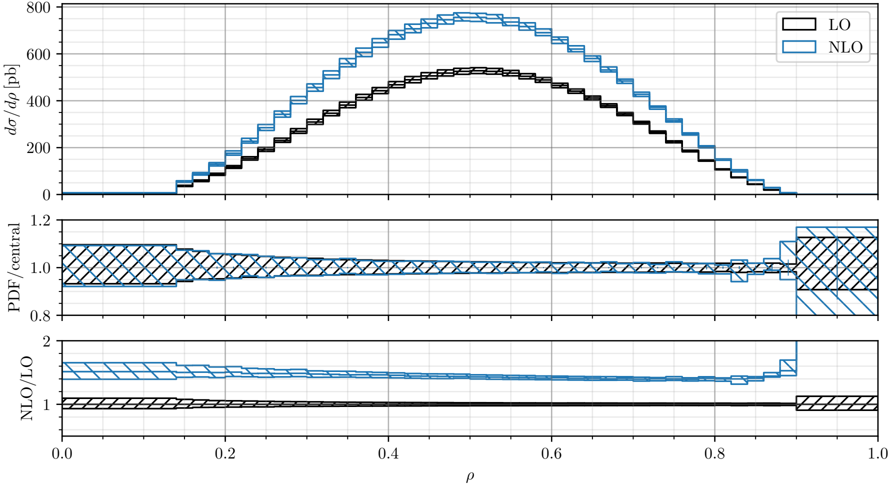

→ very similar size of PDF uncertainty using either a NLO or LO matrix element

NLO PDF uncertainty using $\mu_0 = H_T^B/2$ or $\mu_0 = H_T^B/4$

Predictions of the NLO PDF uncertainty using the CT18NLO PDF set based on a LO partonic cross section and setting either $\mu_0 = H_T^B/2$ or $\mu_0 = H_T^B/4$

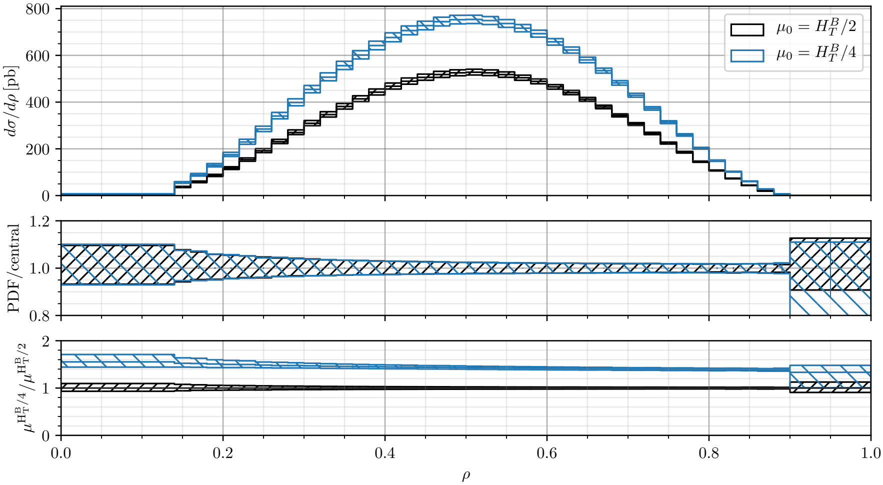

→ very similar size of PDF uncertainty using either dynamical scale

PDF uncertainty in ρ distribution

$\rightarrow$ LO partonic cross section using $\mu_0 = H_T^B/4$

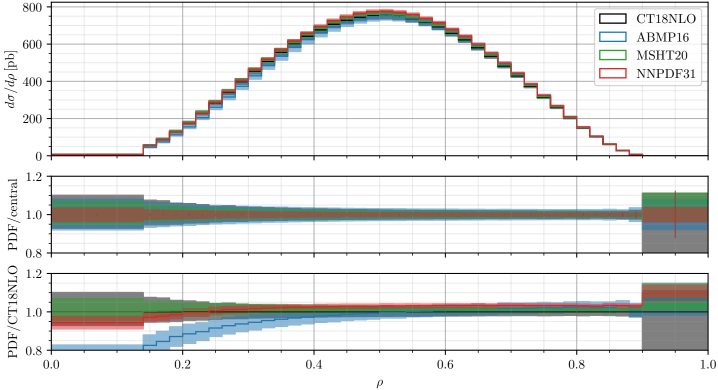

- PDF variation of the order of the scale variation in low ρ tails using the dynamical scale $\mu_0 = H_T^B/4$
- similar behaviour found with all PDF sets in the bulk of the distributions, differences in the high energy tails

Gluon PDF as a function of x

differences between predictions of ρ distribution obtained with different PDF sets found in high energy tails (small ρ) $\rightarrow$ region of large x

$\Rightarrow$ investigate gluon PDF as function of x for $Q^2 = m_t^2$

first bin $\rho \in [0, 0.14]$: peak at $x_{\text{min}} = 0.15$, $x_{\text{max}} = 0.25$

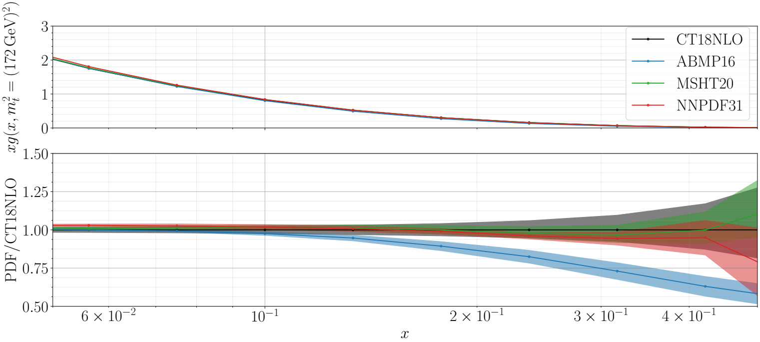

higher values of $\rho \rightarrow$ lower values of x

($\rho \in [0.14, 0.65]$: peak at $x_{\text{min}} = 0.02$, $x_{\text{max}} = 0.07$)

$\Rightarrow$ better agreement between central values of different PDF sets

Conclusions

- dynamical scale preferable to fixed scale:
  (i) smaller width of scale variation uncertainty band in the high-energy tails
  (ii) strongly reduced scale variation uncertainty in normalized ρ distribution
- $\mu_0 \in \{H_T^B/2, H_T^B/4\}$ preferable to $\mu_0 = m_{t\bar{t}j}^B/2$:
  (i) nearly constant differential (NLO/LO) $\mathcal{K}$-factor
  (ii) NLO and LO scale variation bands overlap in low ρ region
  (iii) lower scale variation uncertainty in ρ distribution at NLO
  (here $\mu_0 = H_T^B/4$ preferable to $\mu_0 = H_T^B/2$)
- negligible influence of variation of R-parameter on the scale variation uncertainty using $\mu_0 = H_T^B/2$ or $\mu_0 = H_T^B/4$
- for dynamical scale $\mu_0 = H_T^B/4$ PDF uncertainty becomes as important as scale uncertainty in high-energy tails of the ρ distribution
  (and in the normalized ρ distribution)

Conclusions

- dynamical scale preferable to fixed scale:
  - (i) smaller width of scale variation uncertainty band in the high-energy tails
  - (ii) strongly reduced scale variation uncertainty in normalized ρ distribution
- $\mu_0 \in \{H_T^B/2, H_T^B/4\}$ preferable to $\mu_0 = m_{t\bar{t}j}^B/2$:
  - (i) nearly constant differential (NLO/LO) $\mathcal{K}$-factor
  - (ii) NLO and LO scale variation bands overlap in low ρ region
  - (iii) lower scale variation uncertainty in ρ distribution at NLO (here $\mu_0 = H_T^B/4$ preferable to $\mu_0 = H_T^B/2$)
- negligible influence of variation of R-parameter on the scale variation uncertainty using $\mu_0 = H_T^B/2$ or $\mu_0 = H_T^B/4$
- for dynamical scale $\mu_0 = H_T^B/4$ PDF uncertainty becomes as important as scale uncertainty in high-energy tails of the ρ distribution (and in the normalized ρ distribution)

Thank you for your attention!

Comparing PDF uncertainty and scale uncertainty

calculation of ρ distribution: using CT18NLO PDF set and $\mu_0 = H_T^B/4$, scale uncertainty: NLO partonic cross section and NLO scale variation, PDF uncertainty: LO partonic cross section and NLO PDF variation

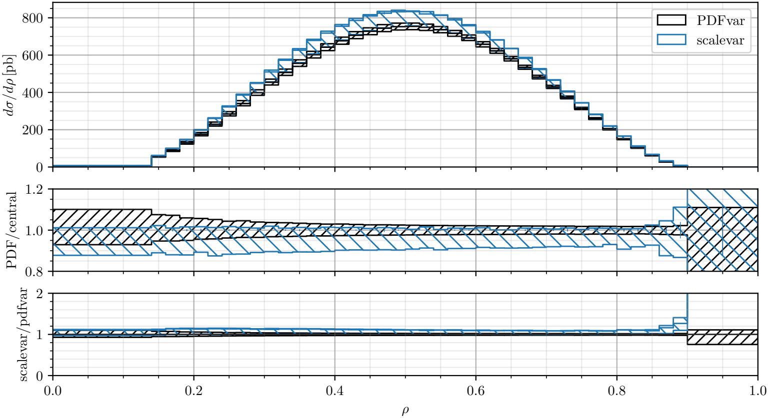

Comparing PDF uncertainty and scale uncertainty

calculation of normalized ρ distribution: using CT18NLO PDF set and $\mu_0 = H_T^B/4$, scale uncertainty: NLO partonic cross section and NLO scale variation, PDF uncertainty: LO partonic cross section and NLO PDF variation

normalization: each scale variation graph by its total cross section and each ρ distribution obtained with different PDF eigenvector by its total cross section

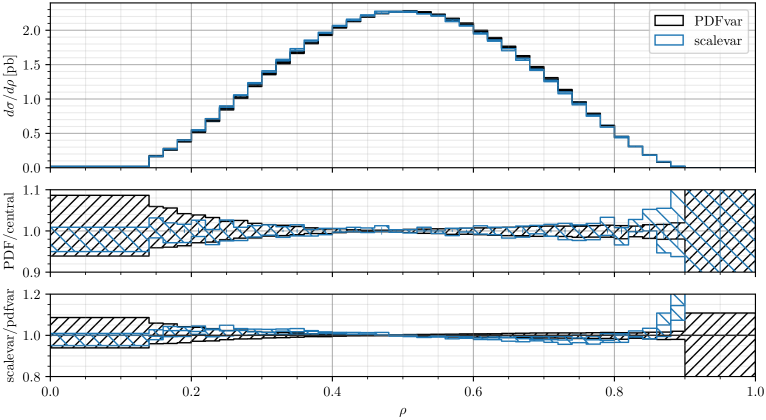

Comparing PDF uncertainty and scale uncertainty

<u>calculation of ρ distribution:</u> using CT18NLO PDF set and $\mu_0 = H_T^B/2$, scale uncertainty: NLO partonic cross section and NLO scale variation, PDF uncertainty: NLO partonic cross section and NLO PDF variation

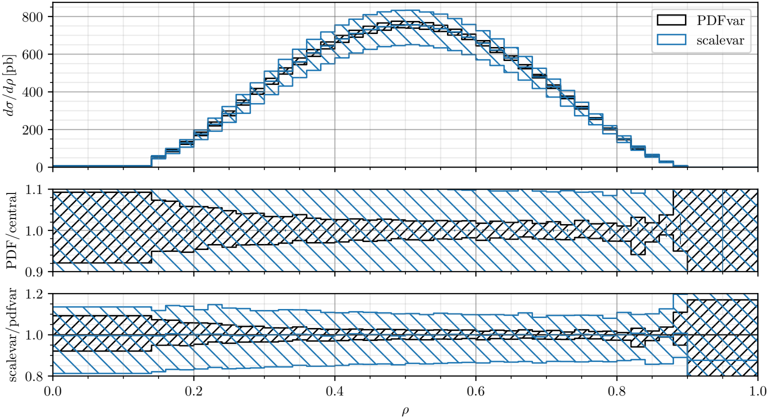

Comparing PDF uncertainty and scale uncertainty

calculation of normalized ρ distribution: using CT18NLO PDF set and $\mu_0 = H_T^B/2$, scale uncertainty: NLO partonic cross section and NLO scale variation, PDF uncertainty: NLO partonic cross section and NLO PDF variation

normalization: each scale variation graph by its total cross section and each ρ distribution obtained with different PDF eigenvector by its total cross section

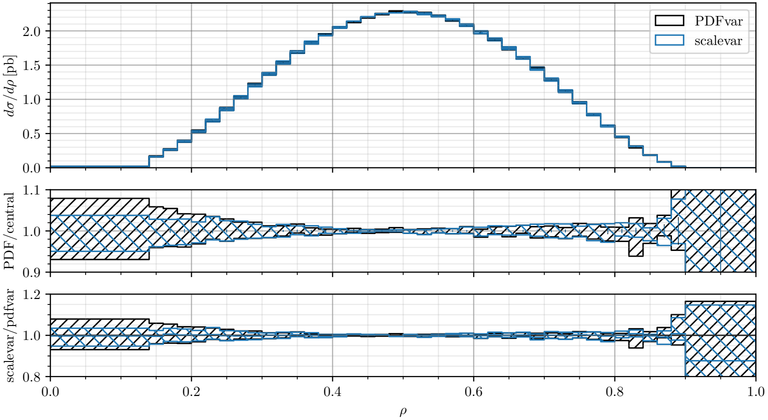

Scale variation in normalized ρ-distribution

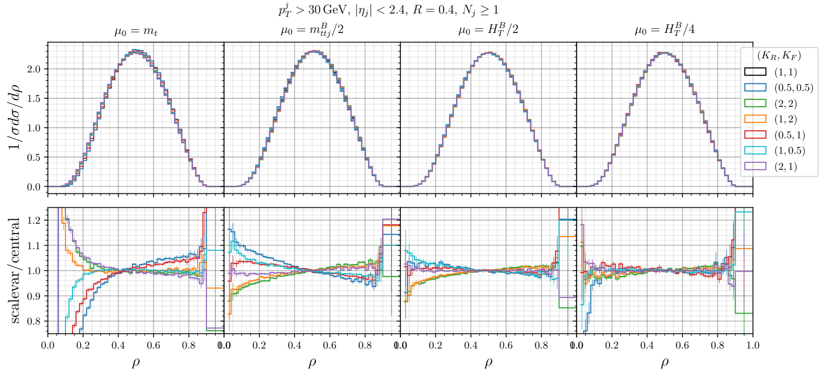

Gluon PDF as a function of x

Observation in ρ distribution at $\rho \sim 1$ for CT18NLO: large uncertainty
Explanation: large statistical uncertainty and increasing PDF uncertainty of CT18NLO compared to ABMP16, MSHT20, NNPDF3.1
smallest x-value: 10^{-3}

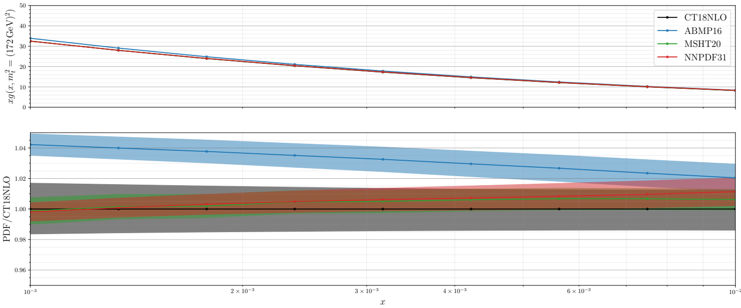

H_T and $m_{t\bar{t}j}$ distributions (real and underlying Born)

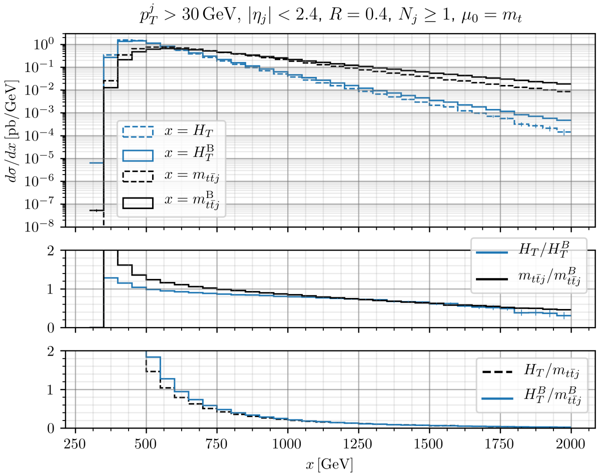

→ harder spectrum of the $m^B_{t\bar{t}j}$ distribution compared to H^B_T distribution

→ softer spectrum of distributions evaluated in real emission configuration, since additional parton carries away energy

Comparison of the p_T^j distribution at NLO and LO

Example: similar behaviour observed in other differential distributions

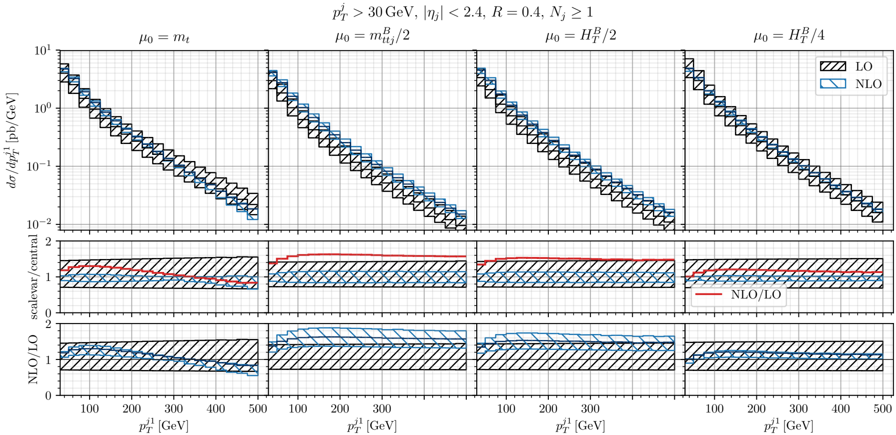

Extraction of the top quark mass through the normalized ρ distribution by the ATLAS collaboration

$m_t^{\text{pole}} = 171.1 \pm 0.4(\text{stat}) \pm 0.9(\text{sys})\,^{+0.7}_{-0.3}(\text{theo})\,\text{GeV}$ (scale: $^{+0.6}_{-0.3}$ GeV, PDF and α_s: ± 0.2 GeV)

$m_t(m_t) = 162.9 \pm 0.5(\text{stat}) \pm 1.0(\text{sys})^{+2.1}_{-1.2}(\text{theo})\,\text{GeV}$ (scale: $^{+2.1}_{-1.2}$ GeV, PDF and α_s: ± 0.4 GeV)

[“Measurement of the top-quark mass in $t\bar{t}+$ 1-jet events collected with the ATLAS detector in pp collisions at $\sqrt{s} = 8$ TeV”, hep-ex/1905.02302]

General jet analysis cuts: $p_T^j > 25\,\text{GeV}$ and $|\eta_j| < 2.5$ reconstructed with the anti-k_T jet clustering algorithm with $R = 0.4$ + additional cuts on separation criteria and cuts on the leptons from the top-quark decay

data unfolded to parton level defined as including initial- and final-state radiation from quarks and gluons before the top-quark decay $\rightarrow$ NLO+PS simulation with cut-off scale of the PS varying on an event-by-event basis

top quark mass extracted through a least-squares method (χ^2 fit)

dominant systematic uncertainties:

- simulation uncertainties: modelling of the PS and hadronization (0.4 GeV) and colour reconnection (0.4 GeV)
- detector response uncertainties: jet energy scale (0.4 GeV)

total systematic uncertainties ± 0.9 GeV

Technical parameters in the POWHEG BOX

```
ncall1 100000 !  number of calls for initializing the integration grid
itmx1 1 !  number of iterations for initializing the integration grid
(automatically set to 1 for parallel runs, see bbinit.f)
ncall2 200000 !  number of calls for computing the integral and finding upper
bound
itmx2 2 !  number of iterations for computing the integral and finding upper
bound
```

→ 100 parallel runs: 40 M phase space points

```
bornsuppfact 100d0 !  (default 0d0) mass param for Born suppression factor
(generation cut) If < 0 suppfact = 1
```

$$F(p_T^2) = \frac{p_T^2}{p_T^2 + \mathtt{bornsupp}^2}$$

```
withdamp 1 !  (default 0, do not use) use Born-zero damping factor
hdamp 237.8775
```

$$F(k_T^2) = \frac{\mathtt{hdamp}^2}{\mathtt{hdamp}^2 + k_T^2}$$

$$R = R_s + R_f = F(k_T^2)R + (1 - F(k_T^2))R$$

```
bornktmin 0.2d0 !  (default 0d0) kt min at Born level for jet in ttbar+jet
```